Acute infection with the intestinal parasite Trichuris muris has long-term consequences on mucosal mast cell homeostasis and epithelial integrity

Sorobetea, Daniel; Holm, Jacob Bak; Henningsson, Henrietta; Kristiansen, Karsten; Svensson-Frej, Marcus

Published in:
European Journal of Immunology

DOI:
10.1002/eji.201646738

2017

Document Version:
Peer reviewed version (aka post-print)

Acute infection with the intestinal parasite *Trichuris muris* has long-term consequences on mucosal mast cell homeostasis and epithelial integrity

Authors

Daniel Sorobetea[1], Jacob Bak Holm[2], Henrietta Henningsson[1], Karsten Kristiansen[2] and Marcus Svensson-Frej[1]

Affiliations

1. Immunology Section, Department of Experimental Medical Sciences, Medical Faculty, Lund University, Lund, Sweden

2. Laboratory of Genomics and Molecular Biomedicine, Department of Biology, University of Copenhagen, Copenhagen, Denmark

Keywords

Mucosal mast cell, *Trichuris muris*, large-intestinal epithelium, MCPt-1, acute parasite infection

Corresponding author

Marcus Svensson-Frej

Immunology section

BMC D14

SE-221 84 Lund

Sweden

Telephone: +46 46 2223338

Fax: +46 46 2220412

E-mail: marcus.svensson_frej@med.lu.se

Abbreviations

IL = Interleukin

MCPt = Mast cell protease

BrdU = 5-bromo-2’-deoxyuridine

Abstract

A hallmark of parasite infection is the accumulation of innate immune cells, notably granulocytes and mast cells, at the site of infection. While this is typically viewed as a transient response, with the tissue returning to steady state once the infection is cleared, we found that mast cells accumulated in the large-intestinal epithelium following infection with the nematode *Trichuris muris* and persisted at this site for several months after worm expulsion. Mast cell accumulation in the epithelium was associated with the induction of type-2 immunity and appeared to be driven by increased maturation of local progenitors in the intestinal lamina propria. Furthermore, we also detected increased local and systemic levels of the mucosal mast cell protease MCPt-1, which correlated highly with the persistent epithelial mast cell population. Finally, the mast cells appeared to have striking consequences on epithelial barrier integrity, by regulation of gut permeability long after worm expulsion. These findings highlight the importance of mast cells not only in the early phases of infection but also at later stages, which has functional implications on the mucosal tissue.

Introduction

The intestinal epithelium acts as a barrier to invading pathogens, thus being important for host defense and maintenance of homeostasis. Critical for this process is the intestinal immune system, which populates both the lamina propria and the epithelium. Reciprocal interaction between immune cells and the epithelium is of paramount importance as improperly regulated immune responses can result in inflammatory bowel disease (IBD), food allergies and other immune-associated disorders[1-3]. Innate immune cells, granulocytes and mast cells included, are crucial components of this defense as they are often the first to respond to epithelial breach; however, the possible role for granulocytes in maintaining barrier integrity at later stages of immune responses remains unclear.

The murine-specific parasitic nematode *Trichuris muris* has been an invaluable tool to study intestinal immunity for nearly fifty years[4]. Once eggs are ingested, *Trichuris*-larvae hatch and burrow into the large-intestinal epithelium without penetrating the basal lamina, and remain in this niche unless expelled. Acute infections with *T. muris* are characterized by an early innate inflammatory response, accompanied by the induction of adaptive Th2 immunity and subsequent worm clearance[4]. After expulsion, the host immune system undergoes a complex and coordinated homeostatic event whereby inflammation is resolved and the infected tissue returns to steady state; a process characterized by immune contraction, clearance of apoptotic cells and tissue repair. However, little attention has been focused to this latter part of the immune response to *T. muris*.

Utilizing *T. muris*, we have investigated the long-term consequences of acute intestinal nematode infection on innate immunity, specifically granulocytes and mast cells. Mast cells, which are

present only at very low numbers in the large intestine at steady state, accumulated in high numbers after infection, notably in the epithelium, and persisted for several months after worm expulsion. The epithelial mast cells displayed a unique surface phenotype and were relatively long-lived, being maintained by maturation of local progenitors. Furthermore, mast cell-derived proteases were detected both locally and systemically long after pathogen clearance, indicative of the mast cells being activated. Finally, accumulation of epithelial mast cells appeared to have striking consequences on barrier integrity by regulation of gut permeability well after worm expulsion. These findings highlight the importance of granulocytes not only in the early phases of infection but also at later stages, with functional implications on the mucosal tissue.

Results

Accumulation of granular cells in the large-intestinal epithelium upon acute *T. muris*-infection

Granulocytes and mast cells are rapidly recruited to sites of inflammation, notably during parasite infections. We infected C57BL/6 mice with a high dose of *T. muris*-eggs and monitored the accumulation of granular cells in the intestinal mucosa over time. As expected, infection with *T. muris* brought about an increase of granular cells in the large intestine, particularly the epithelium (Figure 1A), the majority of which expressed Siglec-F, a lectin most commonly associated with eosinophils. Upon further assessment of the epithelial granulocytes, two distinct Siglec-F^{+} populations became apparent; one high in both Siglec-F and the integrin CD11b (resembling true eosinophils), and the other intermediate in Siglec-F and negative for CD11b (Figure 1B). Conversely, the Siglec-F^{int} population expressed high levels of the epithelium-associated integrin CD103, whereas all Siglec-F^{hi} cells lacked CD103 (Figure 1B). Neither population displayed phenotypic characteristics pertaining to T cells, B cells, monocytes, macrophages, dendritic cells, natural killer cells or neutrophils (Supporting Information Fig. 1A).

High dose infection with *T. muris* elicits strong type-2 immunity in genetically resistant mouse strains, resulting in worm expulsion between day 14 and 21 post-infection (Figure S1B). We therefore performed a series of experiments to address the recruitment kinetics of the two granular cell populations and noted that they followed distinct patterns of accumulation (Figure 1C). While there was only a modest change in total cell numbers of the large-intestinal lamina propria and epithelium (Supporting Information Fig. 1C), the Siglec-F^{hi} cells increased markedly in the epithelium during infection and peaked at the time of worm expulsion, followed by a slow decline as inflammation abated (Figure 1C). On the other hand, the Siglec-F^{int} cells accumulated towards the end of infection, peaked after worm expulsion had occurred and remained at a stable level for at least two more months (Figure 1C). In the small-intestinal epithelium, by contrast,

there was no accumulation of Siglec-F^{hi} cells post-infection, whereas the Siglec-F^{int} population increased dramatically during infection, but disappeared rapidly after worm clearance (Supporting Information Fig. 1D). We did not observe any remaining worms at these late time points, and as expected did not detect parasite-specific IgG2c serum antibodies that are associated with chronic infections (Supporting Information Fig. 1E). Taken together, the phenotypic and kinetic analyses indicated that the two Siglec-F^{+} populations might represent unique cell types, and perhaps serve different functions.

To conclusively rule out that both populations were eosinophils we infected eosinophil-deficient ΔdblGATA-1 mice[5], and monitored the accumulation of Siglec-F^{+} cells in the large-intestinal epithelium. While we failed to detect any Siglec-F^{hi} cells in the large intestine of ΔdblGATA-1 mice (confirming their eosinophilic identity), the Siglec-F^{int} population accumulated with equal efficiency in ΔdblGATA-1 as in littermate control mice (Figure 1D). Furthermore, we found that the Siglec-F^{int} population expressed c-kit (CD117), the receptor for stem-cell factor, indicating that they might be of mast cell origin (Figure 1D). Consistent with this hypothesis, Siglec-F^{int} CD117^{+} cells also expressed the high-affinity IgE receptor (FcεRIα), and interleukin-33 receptor (IL-33Rα) (Figure 1E), both of which are commonly found on mast cells[6]. To confirm that the Siglec-F^{int} population consisted of mast cells, we isolated CD45^{+} Siglec-F^{int} CD103^{+} CD117^{+} FcεRIα^{+} cells from the large-intestinal epithelium at day 49 post-infection and performed PCR analysis for mast cell protease-1 (*mcpt1*) and *mcpt5* (specific to mucosal and connective-tissue mast cells, respectively[7,8]), as well as eosinophil peroxidase (*epx*). As expected, sorted cells expressed *mcpt1*, but had no detectable *mcpt5* or *epx* mRNA, confirming that these cells were de facto mucosal mast cells (Figure 1F). Finally, to verify their epithelial localization, we stained paraffin-embedded biopsies from the cecal-colonic junction with toluidine blue. There was a distinct accumulation of toluidine-stained cells in the large intestine of infected mice, many of which were

in close proximity to, or in direct contact with, the epithelial layer, corroborating the flow-cytometry data (Supporting Information Fig. 1F). Taken together, these data demonstrate that a population of mucosal mast cells appeared in the large-intestinal epithelium of *T. muris*-infected mice, displaying an unexpected phenotype and accumulation at later stages of infection.

Type-2 inflammation-associated accumulation of epithelial mast cells

We next sought to determine whether the accumulation of epithelial mast cells was a direct response to the presence of *T. muris*-worms, or rather driven by the type-2 response associated with acute *T. muris*-infection. To this end, mice were infected with a low dose of *T. muris*-eggs, which in C57BL/6 mice results in a chronic infection characterized by a strong type-1 response [4]. Interestingly, there was no specific accumulation of epithelial mast cells in mice infected with a low dose of *T. muris*-eggs at day 35 post-infection (Figure 2A), a time point corresponding to the peak of mast cell accumulation during high-dose infection (Figure 1C), despite a robust increase in both eosinophils and neutrophils (Supporting Information Fig. 2A). This suggested that the accumulation of mast cells during high-dose infections likely was an indirect consequence of the strong type-2 response induced upon infection rather than being directly worm-driven.

We[9], and others[10], have shown that chronic *T. muris*-infection causes a shift in microbial communities of the large intestine. However, it remains unknown whether acute *T. muris*-infection can have long-lasting effects on the intestinal microbiota that persist after worm expulsion. Since the composition of the microbiota can have a significant impact on immune cells in the gastrointestinal tract[11], it was plausible that the long-term accumulation of mast cells in the intestinal epithelium was a consequence of altered bacterial populations. We therefore performed 16S ribosomal gene-based sequencing on the fecal microbiota and analyzed the composition of microbial communities over time. As reported[9], chronic infection with *T. muris*

led to massive alterations in bacterial families of the large intestine, notably *Lactobacillaceae* (Figure 2B). By contrast, although minor changes occurred upon acute *T. muris*-infection around the time of worm expulsion, these were quickly restored to normal, whereas the microbiota of chronically infected mice continued to diverge (Figure 2B and S2B). It is therefore unlikely that the persistence of epithelial mast cells is due indirectly to any long-lasting effects of the nematode on the microbiota.

As it appeared that the driving force behind the accumulation of mucosal mast cells was the type-2 response, we next set up ex vivo-cultures of intestinal cells with *T. muris*-derived excretory/secretory (E/S) antigens and measured the secretion of a panel of cytokines associated with type-2 responses, as well as with mast cell maturation. While uninfected mice displayed little to no type-2 cytokines, previously infected mice showed enhanced levels of antigen-specific IL-4, IL-5 and IL-13 in both the large and small intestine at day 49 post-infection (Figure 2C), albeit expectedly with higher levels in the large intestine. The levels of general inflammatory cytokines such as IL-6 and TNF-α were not substantially altered in the large intestine at this time point (Supporting Information Fig. 2C). In addition, there was a clear induction of IL-3 and IL-9 (Figure 2D), both of which have been implicated during mast cell maturation[12,13]. In summary, accumulation of epithelial mast cells is unrelated to infection-induced changes to the intestinal microbiota, but appears to be driven by type-2 inflammation.

Epithelial mast cells are sustained by increased maturation of lamina propria progenitors

Given that mast cells were detected in the large-intestinal epithelium for at least two months after worm expulsion we next wanted to assess whether the cells had accumulated early after infection and persisted long-term, or were continuously recruited and replaced as the response to infection progressed. To this end, we fed mice with the thymidine analog 5-bromo-2'-deoxyuridine (BrdU)

via the drinking water between day 17 and 24 after high-dose infection (thus overlapping with worm expulsion) to allow for BrdU incorporation in dividing cells, and tracked its decay over time (Figure 3A). Approximately half of the epithelial mast cells were labeled with BrdU after one week of administration (Figure 3B). The BrdU-labeled mast cells remained positive for several weeks after BrdU administration, with only a slow decline in the frequency of labeled cells over time (Figure 3B). Nonlinear-regression analysis indicated that the BrdU-labeled epithelial mast cells disappeared rapidly immediately after BrdU withdrawal, but had a highly prolonged survival at later stages in the kinetic (Figure 3C). Considering that the number of epithelial mast cells was stable for several months after pathogen clearance (Figure 1C) this suggests that although relatively long-lived, the epithelial mast cells were to some extent also being continuously replaced by newly recruited cells.

Unlike classical granulocytes, which circulate as mature effector cells, mast cells leave the bone marrow as agranular progenitors and mature in peripheral tissues in response to local factors, predominantly at mucosal sites and the skin. While connective-tissue mast cells are mostly self-maintained, the maturation of mucosal mast cells is largely dependent on T cell-derived IL-9[14,15], which also plays an important role in the protective response to some parasites, including *T. muris*[16]. We hypothesized that the accumulation of epithelial mast cells was a consequence of increased bone marrow output, recruitment and/or differentiation of local progenitors driven by the type-2 response, notably IL-9 (Figure 2D). As mentioned previously, the epithelial mast cells were uniform in their phenotype prompting us to more closely investigate mast cells and their progenitors in the lamina propria. Consistent with previous reports[6,17-20], we could detect a small population of agranular lineage$^-$ CD117$^+$ FcεRIα$^-$ α4β7$^+$ IL-33Rα$^+$ FcγRIII/II$^+$ mast cell progenitors (population “P1a”) in the large-intestinal lamina propria of both uninfected and *T. muris*-infected mice, none of which expressed Siglec-F or CD103 (Supporting Information

Fig.3A). Upon entry into the intestinal mucosa, mast cell progenitors undergo a series of maturation steps (Figure 3D) by first up-regulating FcεRIα and down-regulating α4β7 that is crucial for their entry into the intestinal tissue[21,22]. There was no accumulation of mast cell progenitors in the lamina propria of infected mice post-infection (Figure 3E). Similarly, no increase could be detected in either the bone marrow or spleen, but rather a decrease (Supporting Information Fig. 3B). By contrast, in infected mice, a vast majority of the intestinal progenitors had given rise to partially granular FcεRIα^{+} α4β7^{-} mast cells (population "P2b" in Supporting Information Fig. 3A), peaking in number at day 21 post-infection (Figure 3F), i.e. prior to the accumulation of mast cells in the epithelium (Figure 1C). Similar to epithelial mast cells, lamina propria mast cells remained elevated in number after worm clearance (Figure 3F). Consistent with the possibility that lamina propria mast cells can be further activated during infection, a proportion of the cells ("P2b") became Siglec-F^{+} CD103^{+} (Figure 3G), resembling the phenotype of epithelial mast cells. This suggests that instead of an accumulation of circulating progenitors, local mast cell progenitors were giving rise to more mature cells after infection leading to the observed increase in epithelial mast cells.

Altered epithelial permeability after acute *T. muris*-infection

Mast cells have been implicated in the generation of type-2 responses against several parasites[23], including *T. muris*[24]. However, as the bulk of epithelial mast cells accumulated after expulsion we hypothesized that they might serve additional functions, possibly regulating epithelial barrier function given their localization. Consistent with such a possibility, mast cell-derived proteases (notably including MCPt-1) have been shown to regulate epithelial permeability[25]. As mucosal mast cells are characterized by the specific production of MCPt-1, we measured the levels of MCPt-1 locally in the large intestine, distally in the small intestine, as well as systemically in the serum. Although absent in uninfected mice, serum concentrations of MCPt-1

increased dramatically during infection and remained elevated throughout the experimental kinetic (Figure 4A). We did not detect any substantial MCPt-1 secretion by cells isolated from the small intestine (Supporting Information Fig. 4A), nor by cells from the large-intestinal lamina propria at day 49 post-infection (Figure 4B). By contrast, high levels of MCPt-1 were secreted by cells isolated from the large-intestinal epithelium (Figure 4B), correlating with the mature granular phenotype of epithelial mast cells (Figure 1A and S4B). The serum levels of MCPt-1 correlated strongly with the frequency of mast cells in the large-intestinal epithelium regardless of time point post-infection, as determined by Spearman-correlation analysis (Figure 4C). Furthermore, as there was no prolonged accumulation of mast cells at other mucosal sites, such as the small intestine (Supporting Information Fig. 1C) or lungs (data not shown), it is likely that the elevated serum levels of MCPt-1 at later stages in the kinetic derive from large-intestinal mast cells, although we cannot exclude a possible contribution from mast cells at other peripheral tissues.

To address the role of mast cells on intestinal permeability post-infection we gave repeated intraperitoneal injections of either depleting anti-CD117[16,26], or isotype-control antibodies, and measured the uptake of FITC-dextran administered by oral gavage at day 49 post-infection (Figure 4D). Interestingly, previously infected mice had higher serum levels of FITC-dextran than their uninfected counterparts (Figure 4E), consistent with increased intestinal permeability in response to prior infection. Strikingly, despite only a partial reduction of large-intestinal mast cells (Supporting Information Fig. 4C), this effect was reversed in mice treated with anti-CD117 (Figure 4E). Importantly, the increased permeability after infection correlated with increased serum levels of MCPt-1, which were also reduced following mast cell depletion (Figure 4F). Taken together, these results suggest that mast cells accumulating in the large intestine in response to *T. muris* infection may have functional implications on intestinal barrier integrity, and that this effect appears to persist long after the infection has been cleared.

Discussion

Here, we demonstrate that acute *T. muris*-infection leads to the accumulation of a long-lived mast cell population in the large-intestinal epithelium. This accumulation was associated with induction of a type-2 response, and correlated with increased levels of the mucosal mast cell-specific protease MCPt-1 in the serum and locally in the intestine, as well as increased epithelial permeability, suggesting that prior infection may have long-lasting consequences on the local environment as well as influence on subsequent responses.

Mast cells have previously been shown to localize to epithelial surfaces in several models of intestinal inflammation[7,26]. For example, infection with the small-intestinal nematode *T. spiralis* induces a robust accumulation of mast cells in the jejunal epithelium during active infection[7]. Similarly, mice that transgenically overexpress IL-9, systemically[16,26] or restricted to the intestinal epithelium (iFABPp-IL-9Tg mice)[27], have increased numbers of mast cells in the small-intestinal epithelium. In contrast to our findings in the large-intestinal epithelium during *T. muris*-infection however, *T. spiralis*-infection fails to cause epithelial mastocytosis beyond expulsion of the parasite[7]. The reasons for this disparity could be several, and could be linked to the different nature of the small and large intestine, or relate to differences between infection models. Although one may suspect regional differences in microbiota composition to be involved, our data suggest that changes to microbial communities most likely play little part in the accumulation of epithelial mast cells. Instead, our results indicate that induction of type-2 immunity is crucial in driving epithelial mast cell accumulation. Thus, we failed to detect epithelial mast cells following type 1-dominated low-dose *T. muris*-infection. By contrast, high-dose infection with *T. muris* resulted in mast cell accumulation associated with high levels of type-2 cytokines in the large-intestinal lamina propria.

The earliest mast cell progenitors in the lamina propria have been described as agranular CD117$^+$ FcεRIα$^-$ α4β7$^+$ IL-33Rα$^+$ FcγRIII/II$^+$ cells[6,17-20]. Under the influence of local factors, these cells up-regulate FcεRIα while down-regulating α4β7[6]. Our results suggest that a proportion of these cells can go through additional maturation steps in response to infection, characterized by induction of Siglec-F and CD103, translocation to the intestinal epithelium and acquisition of a more granular appearance (summarized in Figure 3D). Interestingly, while we detected dramatically increased numbers of epithelial mast cells, there was no accumulation of mast cell progenitors in the lamina propria. These data are consistent with those observed in iFABPp-IL-9Tg mice, where intestinal mastocytosis occurred despite unchanged numbers of mast cell progenitors[27], and suggest that accumulation relies on increased maturation and/or survival rather than recruitment of progenitors. While the factors that promote induction of epithelial mast cells remain to be identified, it is interesting to note that TGFβ has been implicated in regulation of several aspects of mast cell biology, including expression of CD103 and MCPt-1[28,29]. CD103 (the integrin αE) pairs with β7, together forming the ligand for E-cadherin that is expressed by intestinal epithelial cells, and might therefore facilitate the interaction between mast cells and the epithelium. Thus, we hypothesize that TGFβ could be one of the important factors that promote transition of lamina propria mast cells into their epithelial counterpart.

The observation that epithelial mast cells are uniformly positive for Siglec-F is to our knowledge the first report on expression of this receptor by mast cells. Thus, expression of Siglec-F has been documented on murine eosinophils, and now on mast cells, similar to its human ortholog Siglec-8[30]. In addition, Siglec-F expression has also been described on alveolar macrophages[31], intestinal epithelial tuft cells[32], as well as on a subpopulation of CD11b$^+$ CD103$^+$ dendritic cells in the small intestine (our unpublished observation).

While our BrdU experiments indicated that the epithelial mast cells had a relatively short lifespan immediately after expulsion, $BrdU^+$ cells displayed a much longer half-life at later stages after infection. A possible explanation for this pattern may be the timing of BrdU-administration, which took place during the peak inflammatory response and overlapping with worm expulsion (complete at day 21 post-infection). Hence, mast cells labeled at the early stages of BrdU-administration, prior to worm expulsion, will likely have encountered parasite-derived antigens, cellular debris from damaged epithelial cells and a more inflamed tissue in general. In contrast, mast cells that developed and were labeled after parasite expulsion might have been exposed to a less inflamed environment, which could reflect on their lifespan.

Mast cells have been implicated in regulation of epithelial barrier function[25,27,33], at least in part via release of MCPt-1[25]. Therefore, given the sustained presence of mast cells in the epithelium, as well as the high levels of MCPt-1 in the serum, we assessed epithelial permeability by measuring uptake of FITC-dextran in the serum upon oral administration in mice injected with anti-CD117 antibodies. Similar to our observations in mice following chronic *T. muris*-infection (unpublished observation), previously infected mice had more permeable intestines. Interestingly, despite only partial mast cell depletion following antibody-treatment, we observed a robust reduction in permeability following anti-CD117 injections, consistent with a role for mast cells in regulating epithelial barrier integrity. While the underlying mechanism remains to be established it may be related to regulation of the tight-junction protein occludin, which has been identified as a target of mast cell-derived proteases[25], or via activation of protease-activated receptor-2 by mast cell-derived tryptases, which have been demonstrated to regulate tight-junction integrity[34].

The consequences of increased epithelial permeability associated with long-term epithelial mastocytosis remain to be investigated. Increased leakiness at epithelial surfaces, particularly in the gastrointestinal tract, is linked to higher risk of developing IBD[35] and food allergies[36]. Indeed, although infection with some parasites has proven beneficial in treating various murine models of IBD[37,38], the data on *T. muris* (including our unpublished data) seem to suggest the opposite[39]. Furthermore, whether the long-term effects observed have any bearing on the risk of developing food allergies remains to be determined. Interestingly, several reports strongly link overexpression of IL-9, intestinal mastocytosis and increased epithelial permeability to a predisposition to oral-antigen hypersensitivity[22,27], and *vice versa* in IL-9-deficient mice[40], suggesting that mice that have undergone acute *T. muris*-infection could be more prone to develop food allergy. Finally, our preliminary data suggest that acute *T. muris*-infection might also have systemic consequences. Thus, we observed effects on both the number and phenotype of granulocytes in the lungs, as well as on the local cytokine environment (data not shown). In addition, if the observed epithelial leakiness is indeed due to circulating MCPt-1, one might expect to see similar effects on the lung epithelium, which could have consequences on the outcome of allergic challenge also at this site.

In summary, acute *T. muris*-infection results in accumulation of a population of long-lived mucosal mast cells in the large-intestinal epithelium. Epithelial mastocytosis appears to be associated with type-2 responses, and have long-lasting consequences on the intestinal environment, including regulation of epithelial barrier permeability.

Materials and methods

Mice

C57BL/6 mice were obtained from ENVIGO (An Venray, Netherlands). ΔdblGATA-1 mice were bred in the BMC barrier facility, Lund University, and were a kind gift from Professors Alison Humbles (MedImmune, LLC, Gaithersburg, U.S.A.) and Avery August (Cornell University, Ithaca, U.S.A.). Experiments were conducted with age-matched male/female mice (6-8 weeks old), in strict accordance with animal welfare laws determined by Swedish authorities (Swedish Board of Agriculture, Act 1988:534). The protocol was approved by Malmö/Lund Ethical Board for Animal Research, Lund/Malmö, Sweden (permit: M14-16), and all efforts were made to minimize animal suffering.

Trichuris muris

T. muris (strain E) was maintained as previously described[41]. Mice were infected with a high (350-400) or low (20) dose of eggs in sterile-filtered (0.2μm) tap water by oral gavage to obtain acute or chronic infection, respectively. To assess the worm burden of infected mice, large intestines were excised and frozen at -20°C. Intestines were opened longitudinally upon analysis, and scraped free of worms that were counted under a reverse phase-contrast microscope.

Parasite-derived antigens

Mice of a susceptible strain were infected with approximately 150 *T. muris*-eggs and killed six weeks later. Large intestines were excised, opened longitudinally and rinsed thrice with sterile Dulbecco's phosphate-buffered saline (DPBS; Thermo-Fisher Scientific) supplemented with 500U/ml penicillin + 500μg/ml streptomycin (Thermo-Fisher Scientific). Adult worms were pulled out with forceps, placed in sterile RPMI 1640 (Thermo-Fisher Scientific) supplemented with antibiotics as described above and incubated at 37°C for 20 minutes, followed by a 24-hour

incubation in fresh medium. The medium was collected the following day and centrifuged at 500g for 10 minutes to pellet the eggs. E/S antigens were concentrated in a series of 10-30 minute centrifugation steps in centriprep-centrifugal columns with 10000NMWL (Merck-Millipore) at 2000g, and dialyzed to DPBS in a series of centrifugation steps in Amicon Ultracel-3K Centrifugal Filters with 3000NMWL (Merck-Millipore) at 14000g. The resulting protein concentration was measured by Bradford's assay (280nm) on a SPECTROstar Nano plate reader (BMG Labtech). The antigens were frozen at -80°C.

Tissue preparation and cell isolation

Spleens were mashed in DPBS and passed through 70μm cell strainers (Thermo-Fisher Scientific). Femurs were flushed through with DPBS to obtain the bone marrow, which was homogenized and filtered through 70μm cell strainers. Intestines were stripped of adipose tissue, opened longitudinally and washed thoroughly in DPBS to remove the feces. To isolate immune cells from the large and small-intestinal epithelium, intestines were cut into approximately one cm pieces, and incubated thrice in epithelial-dissociation buffer consisting of Hank's balanced salt solution (HBSS;Thermo-Fisher Scientific) supplemented with 15mM 4-(2-hydroxyethyl)-1-piperazineethanesulfonic acid (HEPES;Thermo-Fisher scientific), 2% fetal bovine serum (FBS; Sigma-Aldrich), 5mM ethylenediaminetetraacetic acid (EDTA;Merck-Millipore), 100U/ml penicillin + 100μg/ml streptomycin, 50μg/ml gentamicin (Thermo-Fisher Scientific) and 1.25μg/ml Fungizone (Thermo-Fisher Scientific) for 15 minutes at 37°C, on continuous shaking. The loosened epithelium was subjected to density-gradient centrifugation using Percoll (GE Healthcare). Briefly, cells were suspended in 40% Percoll and centrifuged over a 70% Percoll layer for 20 minutes, 600g without brake at room temperature. Cells collected between the 40/70 phases were washed with DPBS. To isolate cells from the lamina propria remaining tissue pieces were enzymatically digested in R10 buffer consisting of RPMI 1640 supplemented with 10mM HEPES, 10% FBS, 2mM L-

glutamine (Thermo-Fisher Scientific), 1mM sodium pyruvate (Thermo-Fisher Scientific), 100U/ml penicillin + 100μg/ml streptomycin, 50μg/ml gentamicin and 1.25μg/ml Fungizone, along with 0.3Wünsch-units/ml liberase TM (Roche), 30μg/ml DNase I (Roche) and 5mM $CaCl_2$ for 45 minutes at 37°C with magnetic stirring. The resulting cell suspensions were filtered through 100μm cell strainers (Fisher Scientific), and subjected to density-gradient centrifugation as described above. Lung cells were obtained by first perfusing the mice with DPBS; lungs were subsequently excised, minced into small pieces and digested in R10 buffer for 45 minutes at 37°C, on continuous shaking. The resulting cell suspension was filtered through a 70μm cell strainer, and subjected to density-gradient centrifugation as described above. Cells were enumerated using a KX-21N automated hematology analyzer (Sysmex).

Flow cytometry

Cells were fluorescently labeled for 30 minutes on ice with the following antibodies and reagents: AF700-conjugated mouse (SJL) anti-mouse CD45.2 (clone 104;BioLegend), APC-eF780-conjugated rat anti-mouse CD11b (M1/70;eBioscience), APC-conjugated Armenian hamster anti-mouse FcεRIα (MAR1;BioLegend), PerCP-eF710-conjugated rat anti-mouse CD117 (2B8;eBioscience), PE-CF594-conjugated rat anti-mouse α4β7 (DATK32;BD Biosciences), PE-conjugated rat anti-mouse Siglec-F (E50-2440;BD Biosciences), FITC-conjugated rat anti-mouse Ly-6G (1A8;BD Biosciences), BV786-conjugated rat anti-mouse CD103 (M290;BD Biosciences), BV711-conjugated rat anti-mouse FcγRIII/II (93;BioLegend), BV650-conjugated rat anti-mouse I-A/I-E (M5/114.15.2;BD Biosciences), BV605-conjugated rat anti-mouse CD3 (17A2;BD Biosciences), rat anti-mouse CD19 (1D3;BD Biosciences), and mouse (CH3xBALB/c) anti-mouse NK1.1 (PK136;BD Biosciences), BV421-conjugated rat anti-mouse IL-33Rα (DIH9;BioLegend) along with Aqua-Live/Dead (Thermo-Fisher Scientific) according to manufacturer's instructions. Cells were analyzed on an LSR II flow cytometer (BD Biosciences), and data analyzed with FlowJo software v9.7 (Tree Star Inc.).

Ex vivo-cell stimulations and protein analyses

For cytokine secretion analyses, cells were suspended in R10 buffer, seeded at $2.5x10^6$cells/ml in TC-MicroWell 96U-Nunclon plates (Thermo-Fisher Scientific), and incubated with 25μg/ml E/S antigens for 48 hours at 37°C, 5% CO_2. Cell-free supernatants were collected and frozen at -20°C for subsequent analyses. Cytokines were measured with cytometric bead array (BD Biosciences) according to manufacturer's instructions with the following modification: the amount of capture beads, detection reagents and sample volumes was scaled down five-fold. Data was collected on an Accuri (BD Biosciences) and analyzed with FCAP array v3.0 (SoftFlow Inc.). For MCPt-1 secretion analyses, cells were suspended in R10 buffer, seeded at 10^6cells/ml in TC-MicroWell 96U-Nunclon plates (Thermo-Fisher Scientific), and incubated for 30 minutes at 37°C, 5% CO_2. MCPt-1 was measured using a commercial ELISA kit (eBioscience) according to manufacturer's instructions with the following modification: standard and sample volumes were reduced to 50μl/well. E/S-specific antibodies were measured by a standard ELISA with biotin-conjugated anti-mouse IgG2c antibodies (RMG2a-62;BioLegend), and HRP-conjugated streptavidin (BioLegend).

Mast cell depletion

Anti-CD117 antibodies were generated from a hybridoma (clone;ACK2); a kind gift from Professor Kathryn Else (University of Manchester, Manchester, U.K.). Once confluent, hybridomas were cultured in growth medium containing 2% FBS to minimize non-specific immunoglobulins. IgG antibodies were purified on a protein-A/G column and dialyzed to DPBS by consecutive centrifugation and washing steps using Amicon Ultracel-3K Centrifugal Filters (Merck-Millipore). The concentration was determined by Bradford's assay (280nm absorbance) with 1.4 extinction coefficient for IgG. Rat IgG2b isotype control was purchased from BioXcell. Antibodies were

injected intraperitoneally on days 42, 45 and 47 post-infection (0.5mg/mouse for the first injection, and 0.25mg for subsequent time points).

BrdU-incorporation assay

Mice were given 0.8mg/ml BrdU (Sigma-Aldrich) via the drinking water between days 17-24. Cells were isolated at varying time points after BrdU-removal, and BrdU-incorporation measured by staining with FITC-conjugated anti-BrdU antibodies from a commercially available kit (BD Biosciences), according to manufacturer's instructions. Data was collected on an LSR II flow cytometer.

Assessment of intestinal permeability by FITC-dextran feeding

Mice were starved overnight, fed the following morning with 0.4mg/g body weight FITC-dextran (4kDa;Sigma-Aldrich) dissolved in water and sacrificed four hours later. Blood was collected into Microtainer-SST tubes (BD Biosciences) and centrifuged at 12000g for 5 minutes to obtain serum. FITC-dextran measurements were performed using 488±12nm excitation and 525±12nm emission on a Varioskan LUX Multimode-Microplate Reader (Thermo-Fisher Scientific).

Mast cell isolation and validation

Cells were isolated as described from the large-intestinal epithelium of three mice on day 49 post-infection. Approximately 10^4 mast cells were sorted to high purity on a FACSaria II (BD Biosciences) based on surface expression of CD45, CD117, FcεRIα, Siglec-F and CD103, with dead cells excluded by propidium iodide-staining. Sorted cells were centrifuged, suspended in 100μl lysis buffer (Absolutely RNA Microprep Kit;Agilent Technologies) and frozen at -80°C for RNA isolation. RNA was isolated using Absolutely RNA Microprep Kit according to manufacturer's instructions (including optional DNase treatment). cDNA synthesis was performed with SuperScript III First-

Strand Synthesis System (Thermo-Fisher Scientific) according to manufacturer's instructions (using random hexamers). The cDNA was amplified with SsoFast EvaGreen Supermix (Bio-Rad Laboratories) using the following primers (purchased from Eurofins Genomics): *epx* (forward:5'-CCTTTTGACAACCTGCATGA-3', reverse:5'-CCCAGATGTCAATGTTGTCG-3'), *mcpt1* (forward:5'-GCTGGAGCTGAGGAGATT-3', reverse:5'-GGTGAAGACTGCAGGGG-3') and *mcpt5* (forward:5'-GAACTACCTGTCGGCCTGCAG-3', reverse:5'-AGAACCTTCTGGAAGCTCAGG-3').

Microbiota analyses and bioinformatics

Fresh fecal samples were collected and immediately frozen in liquid nitrogen. DNA extraction (NucleoSpin Soil;Macherey-Nagel) and PCR-based library formation and sequencing were performed as described[9]. Raw sequencing data were processed using QIIME including de novo-OTU picking, chimera-checking and taxonomical assignment using the Greengenes database v13.8[42]. Subsequent analyses were performed in R using the packages Vegan[43] and PhyloSeq[44]. Data were filtered for low-abundance OTUs by removal of OTUs present in <three of the samples, or with a relative abundance across all samples of ≤0.005% resulting in 33991±12378 (mean±SD) reads/sample.

Histology

Biopsies (approximately 0.5cm in size) from the cecal-colonic junction were collected in Carnoy's solution (60% ethanol, 30% chloroform, 10% acetic acid) and stored at room temperature until further processed. Tissue pieces were embedded in paraffin by standard histological techniques and cut into 5μm sections using a Leica microtome. Sections were stained with toluidine blue and mounted in standard fashion. Slides were scanned and analyzed with Aperio ImageScope (Leica Biosystems).

Statistical analyses

All statistical analyses were performed using Prism v5.0 (GraphPad software).

Acknowledgements

We would like to express our gratitude to Professor William Agace for constructive comments on the manuscript, and Maja Toft Løvbakke for technical assistance. This work was supported by grants from the Åke Wiberg, OE&Edla Johansson and Clas Groschinsky Foundations (MSF), and the Royal Physiological Society (DS). DS, JBH, HH and MSF performed the experiments and analyzed the data. DS and MSF conceived the project, with guidance from JBH and KK on the microbiota analysis. DS and MSF, with input from JBH and KK, wrote the manuscript.

Conflict of interest

The authors declare no commercial or financial conflict of interest.

References

[1]. **Maloy KJ and Powrie F**. Intestinal homeostasis and its breakdown in inflammatory bowel disease. *Nature*. 2011; **474**:298–306.

[2]. **Miner-Williams WM and Moughan PJ**. Intestinal barrier dysfunction: implications for chronic inflammatory conditions of the bowel. *Nutr. Res. Rev.* 2016:1–20.

[3]. **Perrier C and Corthésy B**. Gut permeability and food allergies. *Clin. Exp. Allergy*. 2011; **41**:20–28.

[4]. **Cliffe LJ and Grencis RK**. The *Trichuris muris* system: A paradigm of resistance and susceptibility to intestinal nematode infection. *Adv. Parasitol.* 2004; **57**:255–307.

[5]. **Yu C**, **Cantor AB**, **Yang H**, **Browne C**, **Wells RA**, **Fujiwara Y and Orkin SH**. Targeted Deletion of a High-Affinity GATA-binding Site in the GATA-1 Promoter Leads to Selective Loss of the Eosinophil Lineage In Vivo. *J. Exp. Med. Exp. Med.* 2002; **195**:1387–1395.

[6]. **Arinobu Y, Iwasaki H, Gurish MF, Mizuno S, Shigematsu H, Ozawa H, Tenen DG, *et al.*** Developmental checkpoints of the basophil/mast cell lineages in adult murine hematopoiesis. *Proc. Natl. Acad. Sci. U. S. A.* 2005; **102**:18105–10.

[7]. **Friend DS**, **Ghildyal N**, **Austen LKF**, **Gurish MF**, **Matsumoto R and Stevens RL**. Mast Cells that Reside at Different Locations in the Jejunum of Mice Infected with *Trichinella spiralis* Exhibit Sequential Changes in their Granule Ultrastructure and Chymase Phenotype. *J. Cell Biol.* 1996; **135**:279–290.

[8]. **Scudamore CL**, **McMillan L**, **Thornton EM**, **Wright SH**, **Newlands GF and Miller HR**. Mast cell heterogeneity in the gastrointestinal tract: variable expression of mouse mast cell protease-1 (mMCP-1) in intraepithelial mucosal mast cells in nematode-infected and normal BALB/c mice. *Am. J. Pathol.* 1997; **150**:1661–1672.

[9]. **Holm JB, Sorobetea D, Kiilerich P, Ramayo-Caldas Y, Estellé J, Ma T, Madsen L, *et al.*** Chronic *Trichuris muris* infection decreases diversity of the intestinal microbiota and concomitantly increases the abundance of lactobacilli. *PLoS One*. 2015; **10**:1–22.

[10]. **Houlden A**, **Hayes KS**, **Bancroft AJ**, **Worthington JJ**, **Wang P**, **Grencis RK and Roberts IS**. Chronic *Trichuris muris* infection in C57BL/6 mice causes significant changes in host microbiota and metabolome: Effects reversed by pathogen clearance. *PLoS One*. 2015; **10**.

[11]. **Hooper LV**, **Littman DR**, **Macpherson AJ and Program MP**. Interactions between the microbiota and the immune system. *Science.* 2012; **336**:1268–1273.

[12]. **Razin E, Ihle JN, Seldin D, Katz R, Paul II, Hein ANN, Caulfield JP, *et al.*** Interleukin 3 : a Differentiation and Growth Factor for the Mouse Mast Cell That Contains Chondroitin Sulfate E. *J. Immunol.* 1984; **132**:1479–1485.

[13]. **Matsuzawa S**, **Sakashita K**, **Kinoshita T**, **Ito S**, **Yamashita T and Koike K**. IL-9 enhances the growth of human mast cell progenitors under stimulation with stem cell factor. *J. Immunol.* 2003; **170**:3461–3467.

[14]. **Ruitenberg EJ and Elgersma A**. Absence of intestinal mast cell response in congenitally athymic mice during *Trichinella spiralis* infection. *Nature*. 1976; **264**:258–260.

[15]. **Licona-Limón P, Henao-Mejia J, Temann AU, Gagliani N, Licona-Limón I, Ishigame H, Hao L, *et al.*** Th9 cells drive host immunity against gastrointestinal worm infection. *Immunity*. 2013; **39**:744–757.

[16]. **Faulkner H**, **Humphreys N**, **Renauld JC**, **Van Snick J and Grencis R**. Interleukin-9 is involved in host protective immunity to intestinal nematode infection. *Eur. J. Immunol.* 1997; **27**:2536–2540.

[17]. **Jamur M and Grodzki A**. Identification and characterization of undifferentiated mast cells in mouse bone marrow. *Blood*. 2005; **105**:4282–4289.

[18]. **Chen C-C**, **Grimbaldeston MA**, **Tsai M**, **Weissman IL and Galli SJ**. Identification of mast cell progenitors in adult mice. *Proc. Natl. Acad. Sci. U. S. A.* 2005; **102**:11408–13.

[19]. **Dahlin JS**, **Heyman B and Hallgren J**. Committed mast cell progenitors in mouse blood differ in maturity between Th1 and Th2 strains. *Allergy Eur. J. Allergy Clin. Immunol.* 2013; **68**:1333–1337.

[20]. **Bankova LG**, **Dwyer DF**, **Liu a Y**, **Austen KF and Gurish MF**. Maturation of mast cell progenitors to mucosal mast cells during allergic pulmonary inflammation in mice. *Mucosal Immunol.* 2014; **8**:1–11.

[21]. **Gurish MF**, **Tao H**, **Abonia JP**, **Arya A**, **Friend DS**, **Parker CM and Austen KF**. Intestinal mast cell progenitors require CD49dbeta7 (alpha4beta7 integrin) for tissue-specific homing. *J. Exp. Med.* 2001; **194**:1243–1252.

[22]. **Chen CY, Lee JB, Liu B, Ohta S, Wang PY, Kartashov AV, Mugge L, *et al.*** Induction of Interleukin-9-Producing Mucosal Mast Cells Promotes Susceptibility to IgE-Mediated Experimental Food Allergy. *Immunity*. 2015; **43**:788–802.

[23]. **Lawrence CE**, **Paterson YYW**, **Wright SH**, **Knight PA and Miller HRP**. Mouse mast cell protease-1 is required for the enteropathy induced by gastrointestinal helminth infection in the mouse. *Gastroenterology*. 2004; **127**:155–165.

[24]. **Hepworth M**, **Danilowicz-Luebert E**, **Rausch S**, **Metz M**, **Klotz C**, **Maurer M and Hartmann S**. Mast cells orchestrate type 2 immunity to helminths through regulation of tissue-derived cytokines. *Proc. Natl. Acad. Sci. U. S. A.* 2012; **109**:6644–6649.

[25]. **McDermott JR**, **Bartram RE**, **Knight PA**, **Miller HRP**, **Garrod DR and Grencis RK**. Mast cells disrupt epithelial barrier function during enteric nematode infection. *Proc. Natl. Acad. Sci. U. S. A.* 2003; **100**:7761–6.

[26]. **Godfraind C**, **Louahed J**, **Faulkner H**, **Vink A**, **Warnier G**, **Grencis R and Renauld JC**. Intraepithelial infiltration by mast cells with both connective tissue-type and mucosal-type characteristics in gut, trachea, and kidneys of IL-9 transgenic mice. *J. Immunol.* 1998; **160**:3989–3996.

[27]. **Forbes EE, Groschwitz K, Abonia JP, Brandt EB, Cohen E, Blanchard C, Ahrens R, *et al.*** IL-9- and mast cell-mediated intestinal permeability predisposes to oral antigen hypersensitivity. *J. Exp. Med.* 2008; **205**:897–913.

[28]. **Miller HR**, **Wright SH**, **Knight PA and Thornton EM**. A novel function for transforming growth factor-beta1: upregulation of the expression and the IgE-independent extracellular release of a mucosal mast cell granule-specific beta-chymase, mouse mast cell protease-1. *Blood*. 1999; **93**:3473–86.

[29]. **Wright SH**, **Brown J**, **Knight PA**, **Thornton EM**, **Kilshaw PJ and Miller HRP**. Transforming growth factor-beta1 mediates coexpression of the integrin subunit alphaE and the chymase mouse mast cell protease-1 during the early differentiation of bone marrow-derived mucosal mast cell homologues. *Clin. Exp. Allergy*. 2002; **32**:315–24.

[30]. **Bochner BS**. Siglec-8 on human eosinophils and mast cells, and Siglec-F on murine eosinophils, are functionally related inhibitory receptors. *Clin. Exp. Allergy*. 2009; **39**:317–324.

[31]. **Feng Y and Mao H**. Expression and preliminary functional analysis of Siglec-F on mouse macrophages. *J. Zhejiang Univ.* 2012; **13**:386–94.

[32]. **Gerbe F, Sidot E, Smyth DJ, Ohmoto M, Matsumoto I, Dardalhon V, Cesses P, *et al.*** Intestinal epithelial tuft cells initiate type 2 mucosal immunity to helminth parasites. *Nature*. 2016; **529**:226–30.

[33]. **Scudamore CL**, **Thornton EM**, **McMillan L**, **Newlands GF and Miller HR**. Release of the mucosal mast cell granule chymase, rat mast cell protease-II, during anaphylaxis is associated with the rapid development of paracellular permeability to macromolecules in rat jejunum. *J. Exp. Med.* 1995; **182**:1871–1881.

[34]. **Jacob C, Yang PC, Darmoul D, Amadesi S, Saito T, Cottrell GS, Coelho AM, *et al.*** Mast cell tryptase controls paracellular permeability of the intestine: Role of protease-activated receptor 2 and β-arrestins. *J. Biol. Chem.* 2005; **280**:31936–31948.

[35]. **Landy J, Ronde E, English N, Clark SK, Hart AL, Knight SC, Ciclitira PJ, *et al.*** Tight junctions in inflammatory bowel diseases and inflammatory bowel disease associated colorectal cancer. *World J. Gastroenterol.* 2016; **22**:3117–3126.

[36]. **Ventura MT, Polimeno L, Amoruso AC, Gatti F, Annoscia E, Marinaro M, Di Leo E, *et al.*** Intestinal permeability in patients with adverse reactions to food. *Dig. Liver Dis.* 2006; **38**:732–736.

[37]. **Elliott DE**, **Setiawan T**, **Metwali A**, **Blum A**, **Urban JF and Weinstock J V.** *Heligmosomoides polygyrus* inhibits established colitis in IL-10-deficient mice. *Eur. J. Immunol.* 2004; **34**:2690–2698.

[38]. **Smith P**, **Mangan NE**, **Walsh CM**, **Fallon RE**, **McKenzie ANJ**, **van Rooijen N and Fallon PG**. Infection with a helminth parasite prevents experimental colitis via a macrophage-mediated mechanism. *J. Immunol.* 2007; **178**:4557–4566.

[39]. **Bhardwaj EK**, **Else KJ**, **Rogan MT and Warhurst G**. Increased susceptibility to *Trichuris muris* infection and exacerbation of colitis in Mdr1a-/- mice. *World J. Gastroenterol.* 2014; **20**:1797–1806.

[40]. **Osterfeld H**, **Ahrens R**, **Strait R**, **Finkelman FD**, **Renauld JC and Hogan SP**. Differential roles for the IL-9/IL-9 receptor alpha-chain pathway in systemic and oral antigen-induced anaphylaxis. *J. Allergy Clin. Immunol.* 2010; **125**:469–476.e2.

[41]. **Wakelin D**. Acquired immunity to *Trichuris muris* in the albino laboratory mouse. *Parasitology*. 1967; **57** (3):515–24.

[42]. **DeSantis TZ, Hugenholtz P, Larsen N, Rojas M, Brodie EL, Keller K, Huber T, *et al.*** Greengenes, a chimera-checked 16S rRNA gene database and workbench compatible with ARB. *Appl. Environ. Microbiol.* 2006; **72**:5069–5072.

[43]. **Oksanen J BF, Kindt R, Legendre P and O'Hara RB.** Vegan: Community Ecology Package. R package version 1.17–10. 2011.

[44]. **McMurdie PJ and Holmes S**. Phyloseq: An R Package for Reproducible Interactive Analysis and Graphics of Microbiome Census Data. *PLoS One*. 2013; **8**.

Figure legends

Figure 1. Accumulation of granular cells in the large-intestinal epithelium after acute *T. muris*-infection

C57BL/6 mice were infected with a high dose of *T. muris-eggs* and monitored over time for accumulation of granular cells in the large intestine.

(A-C) Flow-cytometry analysis of hematopoietic cells and quantification of granular cell populations in the large-intestinal lamina propria and epithelium of **(A)** uninfected and **(A-B)** *T. muris*-infected mice at day 14 post-infection. Data are from a single experiment representative of three experiments with three individual mice/experiment. **(C)** Quantification of Siglec-F^{hi} (top) and Siglec-F^{int} (bottom) cells in the large-intestinal epithelium after infection. Lines depict the mean frequency of cells, with each symbol representing individual mice (n=6-19, from 3-7 individual experiments with 3-5 mice/time point).

(D-E) Flow-cytometry analysis of hematopoietic cells in the large-intestinal epithelium of *T. muris*-infected **(D)** ΔdblGATA-1 and **(D-E)** C57BL/6 mice at day 49 post-infection. Dark gray=isotype control. Data are from a single experiment representative of one (D) and three (E) experiments with 3-5 mice/experiment **(F)** Gene-expression analysis of *mcpt1*, *mcpt5* and *epx* in sorted viable $CD45^+$ Siglec-F^{int} $CD103^+$ $CD117^+$ $Fc\varepsilon RI\alpha^+$ cells from the large-intestinal epithelium of *T. muris*-infected mice at day 49 post-infection. Data are from a single experiment with three pooled mice.

Figure 2. Epithelial mast cell accumulation occurs under type-2 inflammation

(A-B) C57BL/6 mice were infected with a high (acute) or low (chronic) dose of *T. muris-eggs* and monitored for accumulation of granular cells in the large intestine and changes in microbiota composition. **(A)** Identification (left) and quantification (right) of mast cells in the large-intestinal epithelium at day 35 after acute (top) or chronic (bottom) infection. Data are representative of >3 (acute) and one (chronic) and experiment with 3-5 mice/experiment. **(B)** Bar graph depicting the

relative abundance of bacterial families in the colonic microbiota of uninfected and *T. muris*-infected mice at day 49 post-infection (n=5-10), with indicated keys. “Other”=families that were identified at higher taxonomical level, but not at family level. “No match”=unidentified in database. Data represent mean relative abundance from a single experiment with 30 mice/experiment.

(C-D) Cytokines (measured by CBA) from the supernatants of ex vivo-cultured cells (24 hours) isolated from the large (top) and small-intestinal (bottom) lamina propria of uninfected and high dose-infected mice at day 49 post-infection, in the presence or absence of *T. muris*-derived E/S antigens. **(C)** IL-4, IL-5 and IL-13, and **(D)** IL-3 and IL-9 (n=4). ND=not detected. Bars represent mean+SD of 4-5 biological replicates and are from a single experiment representative of two experiments. Data were analyzed with Mann-Whitney U-test comparing E/S-stimulated cells from infected mice with uninfected mice as control. * ($p<0.05$).

Figure 3. Maturation of local mast cell progenitors maintains the epithelial mast cell pool

(A-C) BrdU-incorporation assay evaluating the lifespan of mast cells in the large-intestinal epithelium following infection with a high dose of *T. muris*-eggs. **(A)** Schematic depiction of the experimental setup; mice were infected with *T. muris*, given BrdU via the drinking water between day 17-24 post-infection, and sacrificed at various time points after BrdU administration to assess BrdU decay. **(B)** Representative flow-cytometry plots of $BrdU^+$ mast cells compared to control. **(C)** Logarithmic graph depicting BrdU-decay in epithelial mast cells, with each dot representing the mean frequency of $BrdU^+$ cells (n=3-6). Non-linear regression (black line) with 95% confidence-interval bands (dotted lines) was calculated using a one-phase decay equation. Data are pooled from two individual experiments with 10 mice/experiment.

(D-G) Identification and quantification of mast cell progenitors and mast cells in the large-intestinal lamina propria of mice infected with a high dose of *T. muris*-eggs. **(D)** Schematic

overview of mast cell maturation in the intestinal mucosa. **(E)** Kinetics depicting the frequency of mast cell progenitors (P2 gate in Supporting Information Fig. 3A). **(F)** Identification and quantification of $\alpha4\beta7^{-}$ $CD117^{+}$ $Fc\varepsilon RI\alpha^{+}$ mast cells (from the P1 gate in Supporting Information Fig. 3A) at day 21 post-infection. **(G)** Representative flow-cytometry plots of $\alpha4\beta7^{-}$ mast cells at day 21 post-infection. Data are from a single experiment with 4-5 mice/time point.

Figure 4. Altered epithelial permeability after *T. muris*-infection

(A-C) C57BL/6 mice were infected with a high dose of *T. muris*-eggs and monitored over time for mast cell proteases in the large intestine and serum. **(A)** Serum concentrations of MCPt-1 (measured by ELISA) at various time points after *T. muris*-infection. Bars represent the mean+SD concentration of MCPt-1 (n=4-8), from two individual experiments with 15 mice/experiment. **(B)** Cells were isolated from the large-intestinal lamina propria and epithelium of uninfected and *T. muris*-infected mice at day 49 post-infection and cultured ex vivo, followed by analysis of MCPt-1 in the culture supernatants. Each bar represents the concentration of MCPt-1 in pooled cell suspensions from 4-5 mice. Data are from one representative experiment of two performed. **(C)** Scatter plot depicting the correlation (Spearman's ρ) between the frequency of mast cells in the large-intestinal epithelium and serum levels of MCPt-1. Dots represent individual mice (from two experiments with 15 mice/experiment).

(D-F) Mast cell depletion affects epithelial barrier permeability. **(D)** Schematic depiction of the experimental setup; mice were infected with *T. muris* and administered anti-CD117 or isotype-control antibodies intraperitoneally at three time points post-infection, after which mice were starved overnight, given FITC-dextran orally in the morning and sacrificed four hours later for analysis of FITC-dextran uptake. **(E)** Serum concentrations of FITC-dextran (measured by spectrophotometry). Dots represent individual mice, with the line depicting the mean concentration. Sera from untreated mice were used as blank controls for FITC-dextran

measurements. Data are pooled from two individual experiments with 15 mice/experiment and analyzed with one-way ANOVA and Tukey's post-test for multiple comparison. ** ($p<0.01$), NS (not significant). **(F)** Serum concentration of MCPt-1 (mean±SD, n=10). Data are pooled from two individual experiments with 15 mice/experiment and analyzed with one-way ANOVA and Tukey's post-test for multiple comparison. ** ($p<0.01$), NS (not significant).

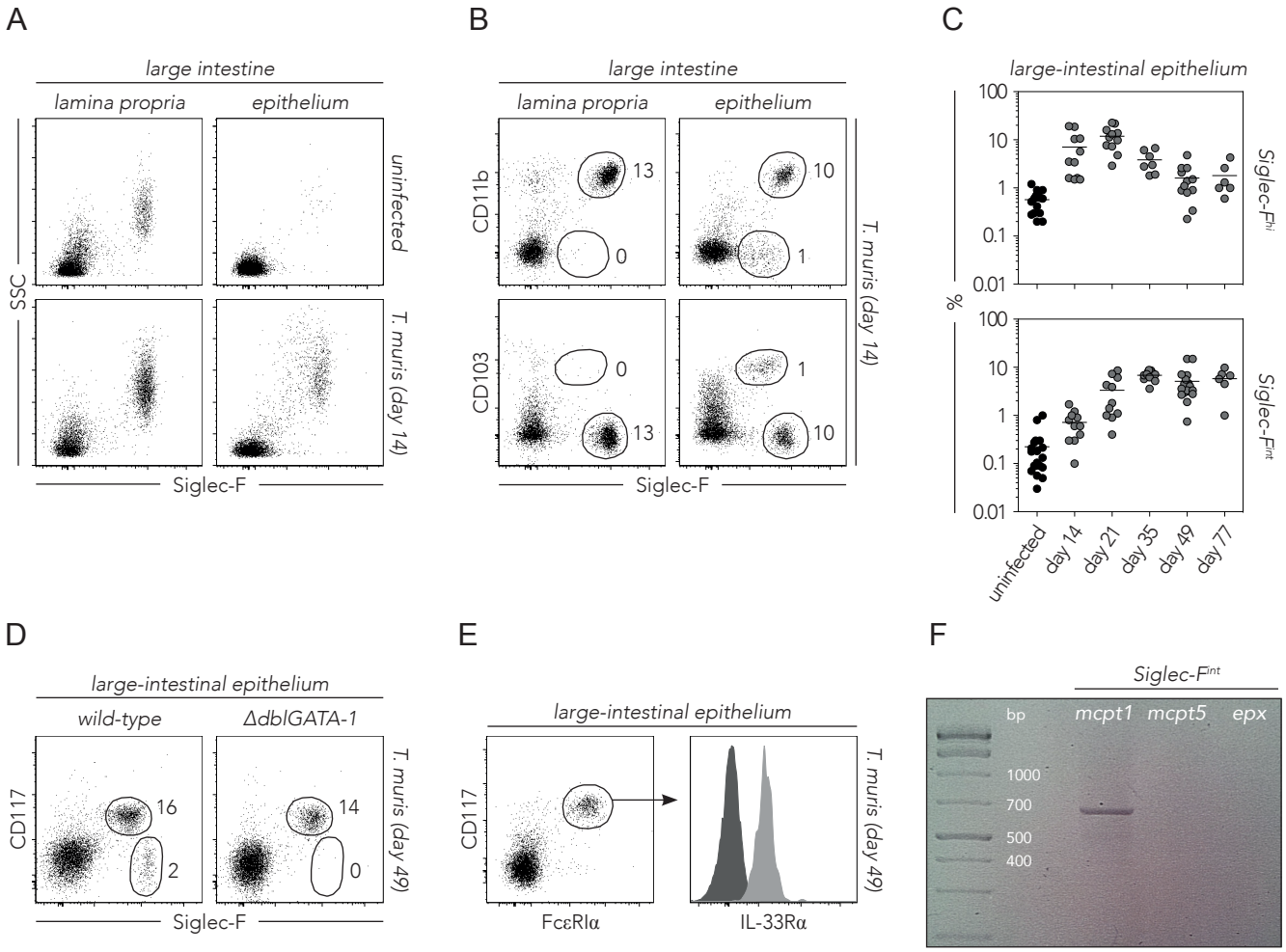
A
large intestine
lamina propria
epithelium
uninfected
T. muris (day 14)
SSC
Siglec-F
B
large intestine
lamina propria
epithelium
CD11b
CD103
13
0
10
1
T. muris (day 14)
Siglec-F
C
large-intestinal epithelium
Siglec-F^hi
Siglec-F^int
%
100
10
1
0.1
0.01
uninfected
day 14
day 21
day 35
day 49
day 77
D
large-intestinal epithelium
wild-type
ΔdblGATA-1
CD117
16
2
14
0
T. muris (day 49)
Siglec-F
E
large-intestinal epithelium
CD117
FcεRIα
IL-33Rα
T. muris (day 49)
F
Siglec-F^int
bp
mcpt1
mcpt5
epx
1000
700
500
400

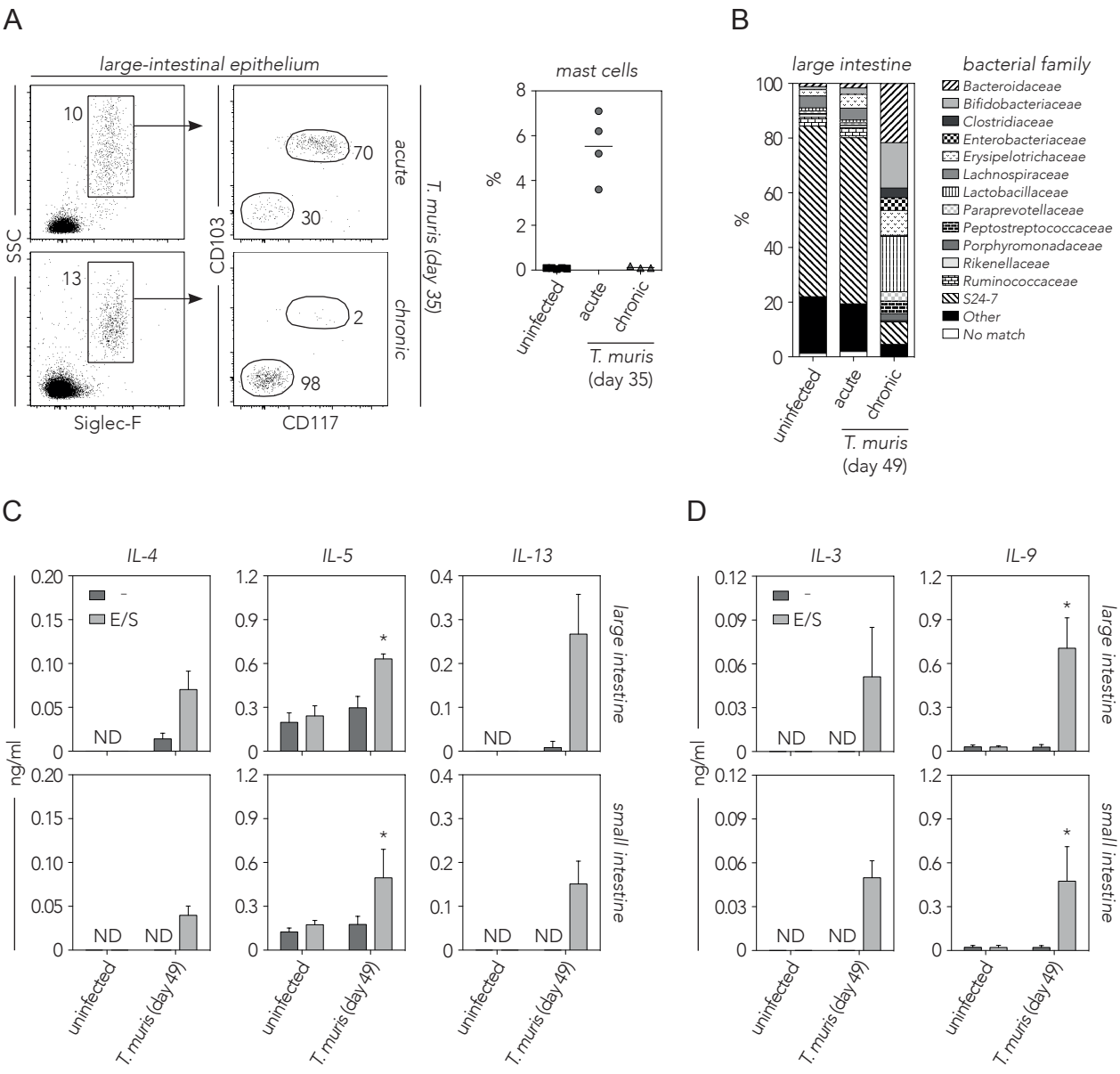
A
large-intestinal epithelium
10
70
30
13
2
98
SSC
CD103
Siglec-F
CD117
acute
chronic
T. muris (day 35)
mast cells
%
uninfected
acute
chronic
T. muris (day 35)
B
large intestine
bacterial family
%
Bacteroidaceae
Bifidobacteriaceae
Clostridiaceae
Enterobacteriaceae
Erysipelotrichaceae
Lachnospiraceae
Lactobacillaceae
Paraprevotellaceae
Peptostreptococcaceae
Porphyromonadaceae
Rikenellaceae
Ruminococcaceae
S24-7
Other
No match
uninfected
acute
chronic
T. muris (day 49)
C
IL-4
IL-5
IL-13
E/S
ND
large intestine
small intestine
ng/ml
uninfected
T. muris (day 49)
D
IL-3
IL-9
E/S
ND
large intestine
small intestine
ng/ml
uninfected
T. muris (day 49)

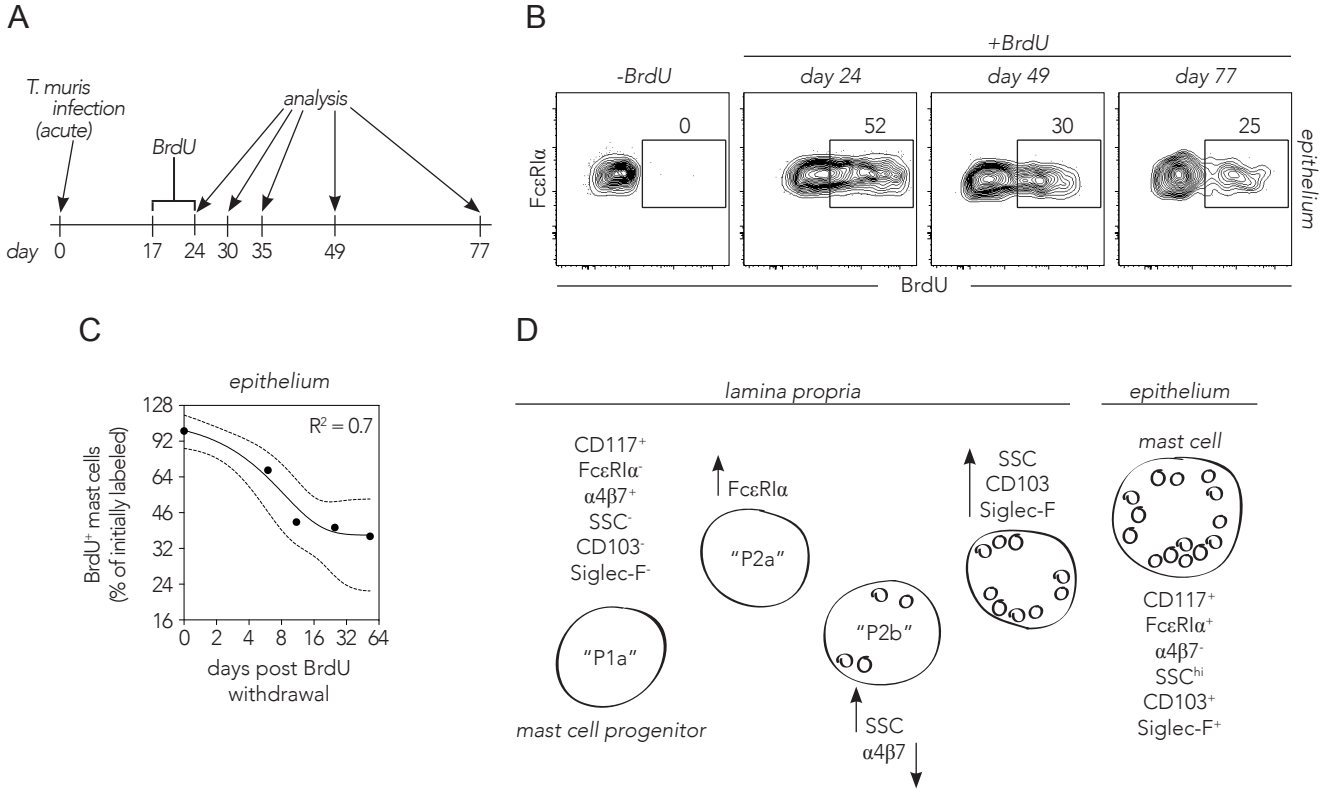
A
T. muris infection (acute)
BrdU
analysis
day 0 17 24 30 35 49 77
B
-BrdU
+BrdU
day 24
day 49
day 77
0
52
30
25
FcεRIα
BrdU
epithelium
C
epithelium
R² = 0.7
BrdU⁺ mast cells (% of initially labeled)
128 92 64 46 32 24 16
0 2 4 8 16 32 64
days post BrdU withdrawal
D
lamina propria
epithelium
CD117⁺ FcεRIα⁻ α4β7⁺ SSC⁻ CD103⁻ Siglec-F⁻
FcεRIα
SSC CD103 Siglec-F
mast cell
"P1a"
"P2a"
"P2b"
mast cell progenitor
SSC α4β7
CD117⁺ FcεRIα⁺ α4β7⁻ SSC^hi CD103⁺ Siglec-F⁺
E
lamina propria mast cell progenitors
%
1 0.1 0.01 0.001
uninfected day 14 day 21 day 35 day 49 day 77
F
"P2b"
%
1 0.1 0.01 0.001
uninfected day 14 day 21 day 35 day 49 day 77
G
"P2b"
uninfected
T. muris (day 21)
CD103
Siglec-F
lamina propria

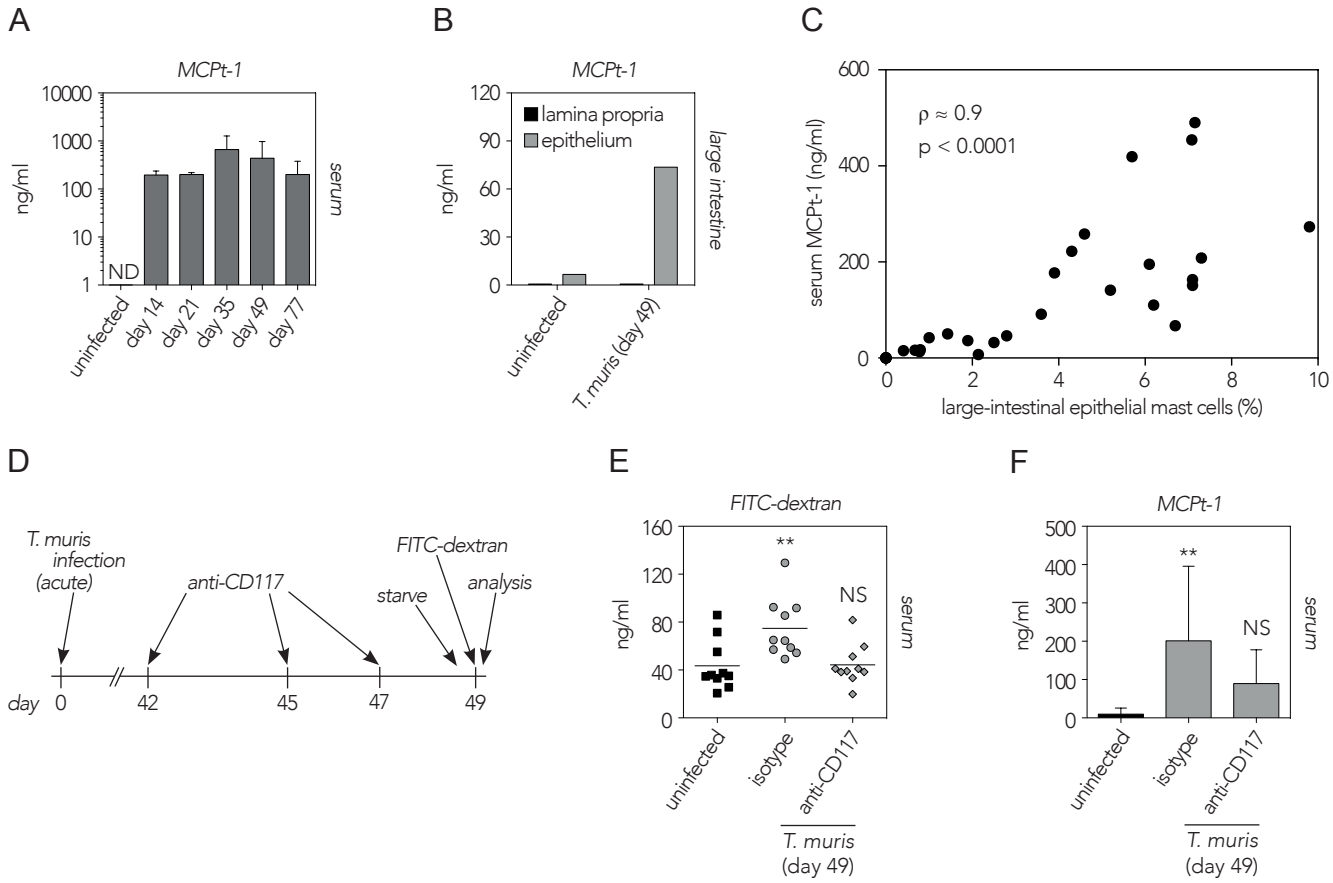
A
MCPt-1
10000
1000
100
10
1
ng/ml
ND
serum
uninfected
day 14
day 21
day 35
day 49
day 77
B
MCPt-1
120
90
60
30
0
ng/ml
lamina propria
epithelium
large intestine
uninfected
T. muris (day 49)
C
600
400
200
0
serum MCPt-1 (ng/ml)
ρ ≈ 0.9
p < 0.0001
0
2
4
6
8
10
large-intestinal epithelial mast cells (%)
D
T. muris infection (acute)
anti-CD117
FITC-dextran
starve
analysis
day 0
42
45
47
49
E
FITC-dextran
160
120
80
40
0
ng/ml
**
NS
serum
uninfected
isotype
anti-CD117
T. muris (day 49)
F
MCPt-1
500
400
300
200
100
0
ng/ml
**
NS
serum
uninfected
isotype
anti-CD117
T. muris (day 49)

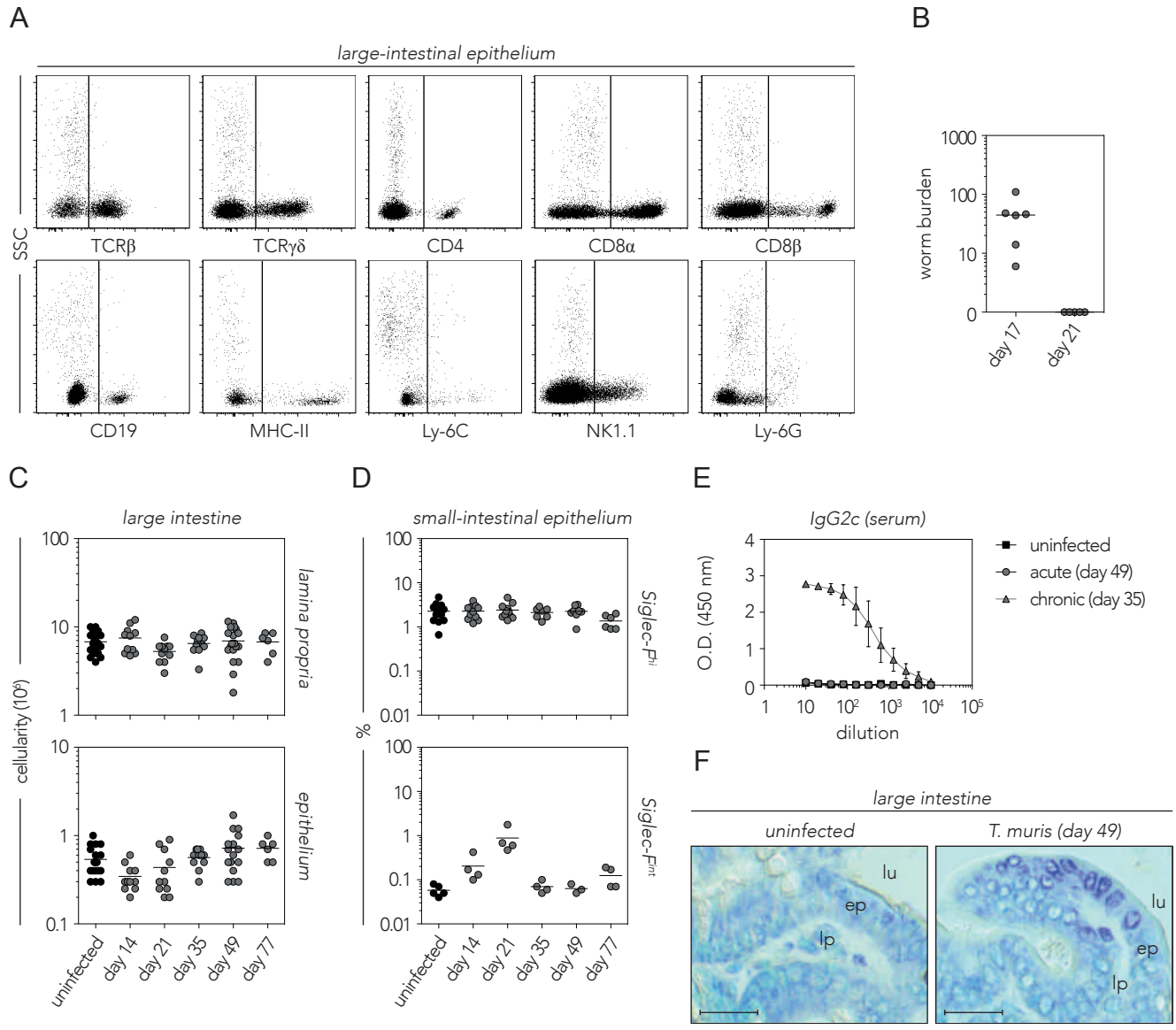
A
large-intestinal epithelium
SSC
TCRβ
TCRγδ
CD4
CD8α
CD8β
CD19
MHC-II
Ly-6C
NK1.1
Ly-6G
B
worm burden
1000
100
10
0
day 17
day 21
C
large intestine
cellularity (10⁶)
lamina propria
epithelium
100
10
1
0.1
uninfected
day 14
day 21
day 35
day 49
day 77
D
small-intestinal epithelium
%
Siglec-F^hi
Siglec-F^int
100
10
1
0.1
0.01
uninfected
day 14
day 21
day 35
day 49
day 77
E
IgG2c (serum)
O.D. (450 nm)
dilution
uninfected
acute (day 49)
chronic (day 35)
F
large intestine
uninfected
T. muris (day 49)
lu
ep
lp

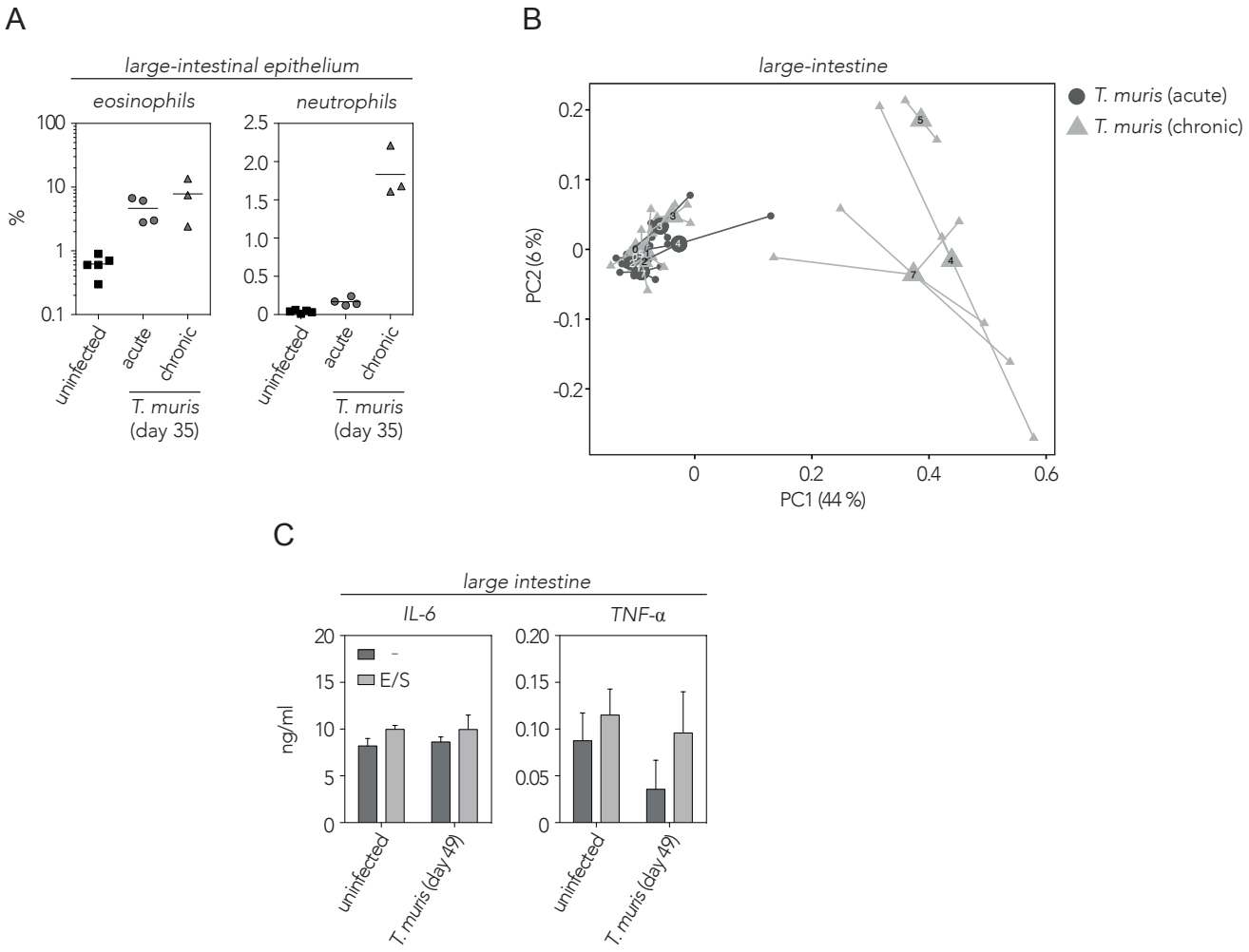
A
large-intestinal epithelium
eosinophils
neutrophils
%
100
10
1
0.1
2.5
2.0
1.5
1.0
0.5
0
uninfected
acute
chronic
T. muris
(day 35)
B
large-intestine
T. muris (acute)
T. muris (chronic)
PC2 (6 %)
PC1 (44 %)
0.2
0.1
0
-0.1
-0.2
0.4
0.6
C
large intestine
IL-6
TNF-α
ng/ml
20
15
10
5
0.20
0.15
0.10
0.05
E/S
uninfected
T. muris (day 49)

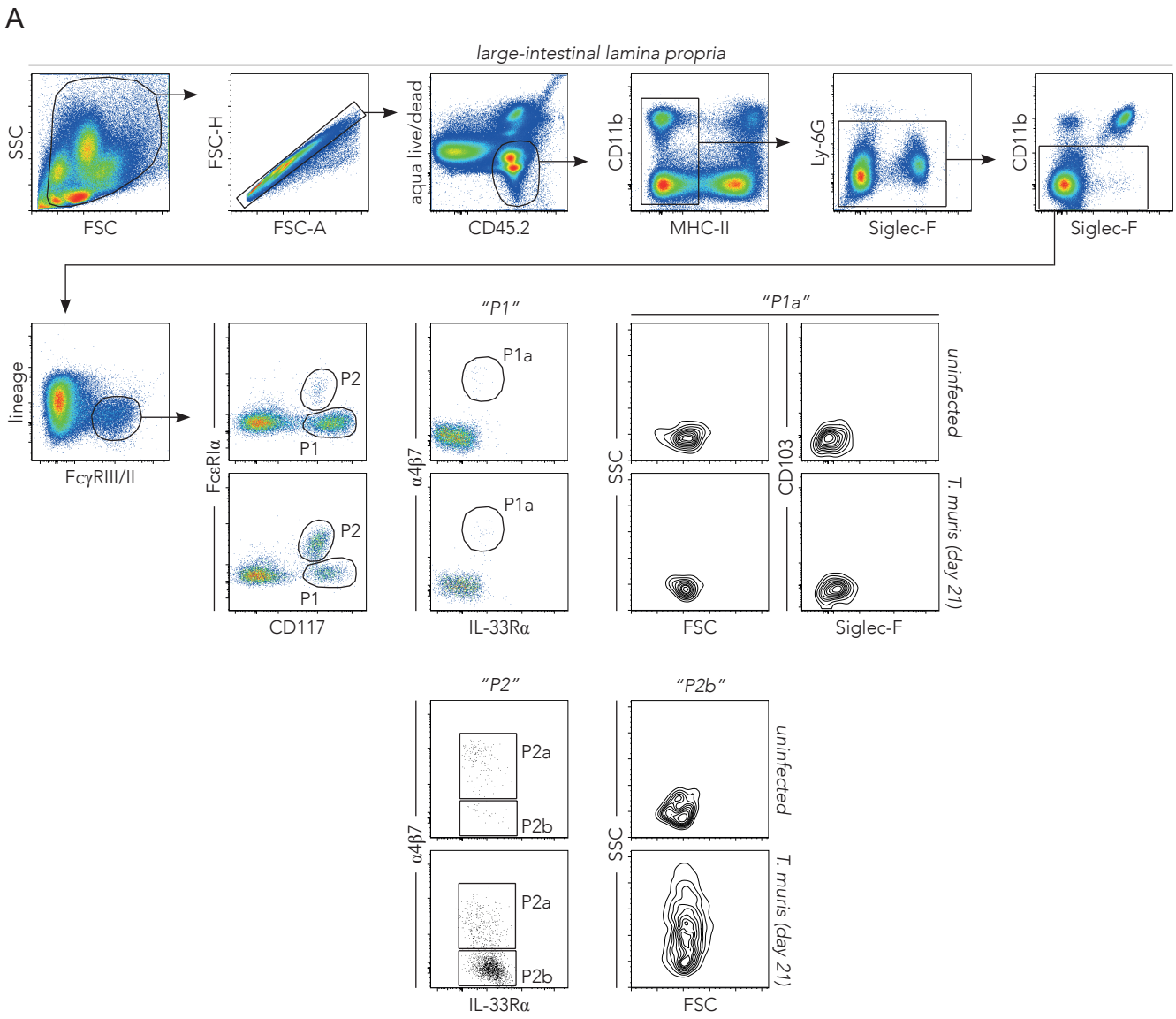
A
large-intestinal lamina propria
SSC
FSC
FSC-H
FSC-A
aqua live/dead
CD45.2
CD11b
MHC-II
Ly-6G
Siglec-F
CD11b
Siglec-F
lineage
FcγRIII/II
FcεRIα
P2
P1
CD117
"P1"
P1a
α4β7
IL-33Rα
"P1a"
SSC
FSC
CD103
Siglec-F
uninfected
T. muris (day 21)
"P2"
P2a
P2b
α4β7
IL-33Rα
"P2b"
SSC
FSC
uninfected
T. muris (day 21)

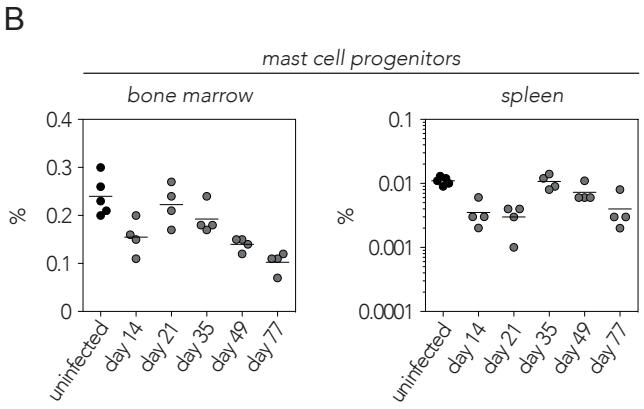
B
mast cell progenitors
bone marrow
spleen
%
0.4
0.3
0.2
0.1
0
0.1
0.01
0.001
0.0001
uninfected
day 14
day 21
day 35
day 49
day 77

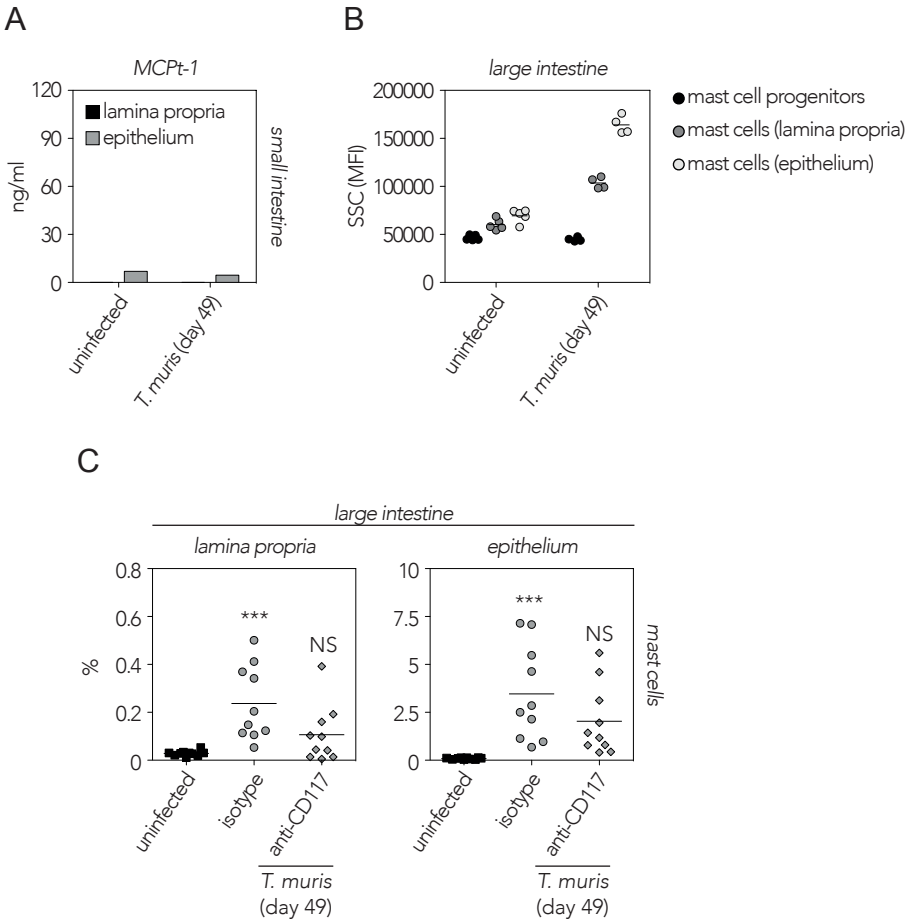
A
MCPt-1
120
90
60
30
0
ng/ml
lamina propria
epithelium
small intestine
uninfected
T. muris (day 49)
B
large intestine
200000
150000
100000
50000
0
SSC (MFI)
mast cell progenitors
mast cells (lamina propria)
mast cells (epithelium)
uninfected
T. muris (day 49)
C
large intestine
lamina propria
epithelium
0.8
0.6
0.4
0.2
0
%
10
7.5
5
2.5
0
***
NS
mast cells
uninfected
isotype
anti-CD117
T. muris
(day 49)